Journal of Neonatal Surgery
ISSN(Online): 2226-0439
Vol. 14, Issue 1s (2025)
https://www.jneonatalsurg.com

OPEN ACCESS

Advanced Hybrid Feature Extraction and DeepLab v3+ Semantic Segmentation for Enhanced Breast Cancer Detection with Cuckoo Search-Optimized Neural Network Classifier

Vishakha Dubey[1], Dr. Shanti Rathore[2], Dr. Rahul Gedam[3]

[1]Research Scholar, Dr. CV Raman University, Kota Bilaspur, India

Email ID: vishakha.dubey1985@gmail.com

[2]Associate Professor, ET & T Department, Dr. CV Raman University, Kota Bilaspur, India

Email ID: rathoreshanti@gmail.com

[3]Associate Professor, ET & T Department, LCIT, Bilaspur, India

Email ID: engg.rahul2801@gmail.com

Cite this paper as: Vishakha Dubey, Dr. Shanti Rathore, Dr. Rahul Gedam, (2025) Advanced Hybrid Feature Extraction and DeepLab v3+ Semantic Segmentation for Enhanced Breast Cancer Detection with Cuckoo Search-Optimized Neural Network Classifier. *Journal of Neonatal Surgery*, 14 (1s), 960-981.

ABSTRACT

This paper introduces a hybrid methodology for enhancing breast cancer detection using thermographic images. The approach combines DeepLab v3+ semantic segmentation with advanced feature extraction techniques, improving classification accuracy. DeepLab v3+ isolates regions of interest (ROIs) from thermograms, focusing on areas likely indicating cancerous lesions. Feature extraction methods like morphological statistical features, Discrete Wavelet Transform (DWT), Local Binary Patterns (LBP), and Enhanced Marine Predator Optimization (EMPO)-Optimized Dual-Tree Complex Wavelet Transform (DTCWT) capture diverse thermal patterns indicative of breast cancer. Principal Component Analysis (PCA) is used for dimensionality reduction, enhancing computational efficiency while preserving important information. The extracted features are classified using a Cuckoo Search-Optimized Neural Network (CSA-NN), which optimizes neural network parameters and addresses class imbalance and feature redundancy. Experimental results demonstrate that this hybrid methodology outperforms traditional techniques, achieving high accuracy, sensitivity, specificity, and precision across breast cancer thermography datasets. The proposed method highlights the potential of combining advanced image processing and machine learning for reliable breast cancer detection.

Keywords: *CSA-NN, DTCWT, DWT, EMPO, LBP, PCA.*

1. INTRODUCTION

Breast cancer continues to be one of the most prevalent and life-threatening diseases affecting women globally, making its early and accurate diagnosis a critical aspect of healthcare. Traditional diagnostic approaches such as mammography and ultrasound, though widely employed, face significant challenges in terms of their sensitivity and specificity. These challenges are particularly pronounced in dense breast tissues or in resource-constrained settings where access to advanced diagnostic tools may be limited. Consequently, there is a growing need for innovative solutions that combine advanced imaging techniques with modern computational methodologies to improve diagnostic accuracy and accessibility.

In recent years, the integration of thermographic imaging with artificial intelligence (AI)-based analytical frameworks has gained considerable attention as a promising alternative for breast cancer detection. Thermography provides a non-invasive, radiation-free imaging modality that detects subtle temperature variations on the skin's surface, which may indicate underlying abnormalities. However, to effectively harness the potential of thermography, robust image processing and classification techniques are essential. Semantic segmentation algorithms, such as DeepLab v3+, and optimized neural networks have emerged as key components in this domain, enabling precise identification of regions of interest (ROI) and accurate classification of breast abnormalities.

This research explores a novel system for breast cancer detection and classification that integrates thermographic imaging with advanced AI techniques. The proposed methodology incorporates state-of-the-art semantic segmentation for precise ROI extraction, comprehensive feature extraction processes for enhanced data representation, and an optimized classification framework powered by neural networks. By addressing the limitations of existing diagnostic methods and introducing innovative computational approaches, the proposed system aims to enhance both the accuracy and efficiency of breast cancer diagnosis.

The motivation for this work stems from the limitations of conventional diagnostic techniques and the underexplored potential of AI-driven thermographic analysis. Traditional imaging methods often struggle with high false-positive rates and reduced efficacy in certain patient populations, leading to unnecessary biopsies and delays in treatment. In contrast, thermography offers the potential for early anomaly detection by capturing functional changes before structural abnormalities are evident. However, its effectiveness depends on advanced segmentation and classification methods to analyze the thermograms accurately.

The key contributions of this paper are as follows:

- ***DeepLab v3+ for Semantic Segmentation:*** This paper employs DeepLab v3+ to address challenges in accurately segmenting regions of interest (ROI) from breast thermographic images. The model's capability to process multi-scale features ensures high precision in detecting tumor regions, even in complex cases.
- ***Hybrid Feature Extraction:*** A unique combination of feature extraction methods, including Discrete Wavelet Transform (DWT), Local Binary Patterns (LBP), and EMPO-optimized Dual-Tree Complex Wavelet Transform (DTCWT), is proposed for a holistic representation of the data. These features encompass statistical, textural, and frequency-domain information critical for accurate classification.
- ***Feature Fusion and Dimensionality Reduction:*** To ensure computational efficiency and reduce feature redundancy, PCA is utilized to fuse and reduce the dimensionality of extracted features while retaining the most significant information.
- ***Cuckoo Search-Optimized Neural Network:*** A neural network classifier optimized by the Cuckoo Search Algorithm (CSA) is implemented to achieve superior classification accuracy. This optimization ensures efficient parameter tuning, resulting in robust performance in diverse datasets.

Through this work, we aim to contribute to the field of computer-aided diagnosis by presenting a system that balances innovation, accuracy, and practicality. The proposed methodology leverages accessible imaging techniques, cutting-edge AI algorithms, and rigorous optimization strategies to address current gaps in breast cancer diagnosis, with the ultimate goal of improving patient outcomes and advancing the state of research in this vital area.

The rest of the paper is structured as follows: Section II reviews the literature on breast cancer detection and diagnosis. Section III outlines the materials and methods used in the paper. Section IV presents the proposed methodology. Section V discusses results and analysis, including performance evaluation on multiple datasets. Finally, Section VI concludes with the findings and potential future directions.

2. LITERATURE REVIEW

The study of breast thermography for detecting lesions has gained significant importance in recent years. Although it is not considered a replacement for current diagnostic techniques, the literature suggests that thermography is a valuable tool for early detection and research into breast lesions. For instance, in a study by [1], the authors compared the accuracy of breast thermography with mammography, involving 132 women aged 24 to 75 at the Tehran Cancer Institute in Iran. Thermograms were categorized using the Marseille system, and analyses were conducted on thermal differences in the images. The study revealed that mammography had a higher accuracy (76%) compared to thermography (69.7%), but they acknowledged the study's limitation due to the small sample size and the inclusion of extreme cases unfavorable for thermography.

In another study [2], thermography was compared with PET-CT. The authors analyzed full-body PET and thermographic images and used K-means clustering to segment different temperature profiles in thermograms, helping to assess breast cancer detection. They concluded that an asymmetric temperature profile in thermograms could be a valuable method for identifying breast cancer.

A separate study [3] focused on 92 patients advised to undergo biopsy after mammography or ultrasound. The study incorporated three scores—general risk, clinical data, and a score based on artificial neural network analysis. This approach successfully identified 58 out of 60 malignant lesions with a 97% sensitivity, 44% specificity, and 82% negative predictive value. The authors concluded that infrared thermography is a beneficial supplementary study for mammography and ultrasound, especially for women with dense breast tissue.

Thermal asymmetry analysis between the left and right breasts has been another method for identifying abnormalities. A study by [4] introduced two classification algorithms using unsupervised learning with K-means and supervised learning

with KNN, based on feature extraction. The authors highlighted the significance of feature extraction in studying breast thermal asymmetry.

Other approaches, such as independent component analysis, have also been applied to breast thermography for automatic cancer detection. For example, [5] used a public database of breast thermograms and applied methods like PCA and Otsu binarization to isolate areas of malignant tissue in thermograms.

In statistical analysis, [6] focused on using image moments and co-occurrence matrices to extract features like energy, homogeneity, and contrast. They applied fuzzy logic to classify thermograms, achieving 80% classification accuracy on a dataset of 150 cases. Additionally, [7] proposed a parametric estimation approach for tumor characteristics, including depth and size, by simulating thermograms and solving the Pennes heat equation using genetic algorithms and finite element methods.

Cancer, being the second leading cause of death globally, with breast cancer constituting a significant portion of cases, demands ongoing research for early detection. In this context, [8] applied artificial neural networks to extract features from breast cancer cell images, achieving 90% classification accuracy. Machine learning, particularly for cancer detection, has proven to be an essential tool in early diagnosis and prediction. The authors of [9] and [10] demonstrated the effectiveness of algorithms like Logistic Regression, Decision Trees, and Support Vector Machines (SVM) for predicting breast cancer recurrence and performing diagnostic classification tasks.

The authors of [11], focused on applying machine learning models to mammogram images and breast cancer datasets. Algorithms like SVM, Decision Trees, Naive Bayes, and Random Forest have shown varying levels of performance in terms of accuracy and classification. In particular, [12] highlighted deep learning's superior performance over traditional machine learning methods, achieving a 94.3% accuracy with convolutional neural networks.

Moreover, [13] used various machine learning methods to predict breast cancer recurrence, where the SVM method provided the highest accuracy. The authors of [14] applied SVM and other methods on mammogram images and found that Support Vector Machines outperformed others with a high accuracy rate of 97.13%. The authors of [15] also worked on early breast cancer diagnosis by applying machine learning techniques to the Wisconsin breast cancer dataset and found that Bayesian Network showed the best performance in terms of sensitivity and precision.

The use of deep learning in breast cancer detection was explored by [16], who achieved a high accuracy rate of 96.44% using convolutional neural networks, outperforming traditional machine learning techniques. In another study, [17] applied various machine learning methods on microarray datasets and achieved high accuracy with SVM, further demonstrating the effectiveness of machine learning models for breast cancer classification. Similarly, [18] worked with microarray datasets to classify cancer data and found that SVM was the most effective model in comparison to others.

Additionally, [19] used tree-based classification models and miRNA expression datasets to determine biomarkers for breast cancer. Their study provided crucial insights into important microRNAs in breast cancer classification, contributing to the development of early detection biomarkers.

- ***Research Gap:*** While significant progress has been made in using thermography and machine learning techniques for breast cancer detection, there is a need for more robust and integrated methodologies that combine the strengths of different imaging techniques with advanced machine learning models. Current approaches often rely on limited datasets or single-modality analyses, which may not fully capture the complexity of breast cancer. Our proposed methodology aims to bridge this gap by integrating thermographic data with advanced machine learning models for more accurate and reliable early diagnosis of breast cancer, thus improving detection rates and reducing false positives/negatives in clinical settings.

3. MATERIALS AND METHODS

3.1 Image Decomposition Using Optimized DTCWT

The Dual-Tree Complex Wavelet Transform (DTCWT) is utilized as a key step in the image processing pipeline for breast cancer detection. It effectively decomposes input images into low and high-frequency components, allowing detailed analysis of both structural and textural patterns. This decomposition aids in preserving critical spatial details and minimizing artifacts.

The input images, denoted as MM_1 and MM_2, are processed using an optimized DTCWT configuration. The optimization, achieved through the Enhanced Marine Predator Optimization (EMPO) algorithm, ensures an optimal number of decomposition levels, balancing computational efficiency and feature extraction precision.

Mathematically, the decomposition of an image $g(s)$ involves convolving it with a low-pass scaling function $\Phi(s)$ and a band-pass wavelet $\psi(s)$. The resulting decomposition can be expressed as:

$$g(s) = \sum_{m=-\infty}^{\infty} d(m)\Phi(s-m) + \sum_{k=0}^{\infty}\sum_{m=-\infty}^{\infty} e(k,m)2^{\frac{k}{2}}\psi(2k^s - m) \quad (1)$$

Where,

- $d(m)$: Scaling coefficients, capturing the low-frequency content of the image, calculated as:

$$d(m) = \int_{-\infty}^{\infty} g(s)\Phi(s-m)ds \quad (2)$$

- $e(k,m)$: Wavelet coefficients, representing the high-frequency details of the image, determined by:

$$e(k,m) = 2^{\frac{k}{2}} \int_{-\infty}^{\infty} g(s)\psi(2^k s - m)ds \quad (3)$$

In this process, the DTCWT employs low-pass filters $(\phi_0(s))$ and high-pass filters $(\psi_1(s))$ in both real and imaginary filter banks. These filters separate the image into its low-frequency components ($MM1_1^{low}$ and $MM1_2^{low}$) and high-frequency components ($MM1_1^{high}$ and $MM1_2^{high}$). The low-frequency components contain the coarse structural details, while the high-frequency components capture fine-grained textural features.

This decomposition stage is pivotal in the hybrid feature extraction process. By isolating significant spatial and textural information, it ensures that the subsequent analysis stages focus on the most relevant characteristics of the input images. Furthermore, the EMPO-based optimization enhances the effectiveness of the DTCWT, ensuring precise and computationally efficient feature extraction for breast cancer detection.

3.2 Low-Frequency Coefficient Fusion Using Max Rule

The Max Rule-based fusion of low-frequency coefficients is a critical step in combining the structural information from the decomposed images. In this process, the low-frequency components of the input images, $MM1_1^{low}$ and $MM1_2^{low}$, are merged by selecting the maximum intensity value for corresponding pixels. This approach ensures that the fused image retains the most significant features from both inputs while minimizing information loss.

The fusion process is mathematically defined as:

$$FM1_{max\_rule}^{low} = \sum_{p=0}^{P} \sum_{q=0}^{Q} Max\left(MM1_1^{low}(p,q) + MM1_2^{low}(p,q)\right) \quad (4)$$

Where:

- $MM1_1^{low}(p,q)$ and $MM1_2^{low}(p,q)$ are the low-frequency coefficient values of the input images at pixel position (p,q).
- $FM1_{max\_rule}^{low}$ is the resultant fused image in the low-frequency domain.
- P and Q represent the dimensions of the images.

This fusion ensures that for each pixel, the highest intensity value from the two input images is preserved, capturing the most relevant structural details.

The schematic representation of this fusion model highlights its simplicity and effectiveness in integrating information from the input images, emphasizing areas with significant low-frequency content while preparing the data for subsequent stages in the image processing pipeline.

3.3 Image Reconstruction by Inverse Optimal DTCWT

The image reconstruction process utilizes the Inverse Optimized DTCWT ($Inv\_OptDTCWT$) to rebuild the fused image from its decomposed high and low-frequency components. The reconstruction process is mathematically represented by:

$$IR_1(RM1^{high}, RM1^{low}) = Inv\_OptDTCWT\left(FM1_{fuzzy}^{high}, FM1_{max\_rule}^{low}\right) \quad (5)$$

Where:

- IR_1 is the reconstructed image.
- $RM1^{high}$ and $RM1^{low}$ represent the high and low-frequency components of the reconstructed image.
- $FM1_{fuzzy}^{high}$ and $FM1_{max\_rule}^{low}$ are the high and low-frequency fused images obtained from the previous stages.

This process ensures that the final fused image preserves both the detailed high-frequency features and the structural low-frequency features.

3.4 Proposed EMPO Algorithm

The Enhanced Marine Predators Optimization (EMPO) algorithm is introduced to overcome limitations of the conventional MPO algorithm, enhancing convergence rates and handling optimization challenges effectively. EMPO is used to optimize parameters like the number of decomposition levels in DTCWT and hidden neurons in DNN for better fusion performance. The position update of prey in EMPO is computed as:

$$\vec{Ri} = \frac{\left((Fd*2)+Pi\right)Tc}{Npp} \quad (6)$$

Where:

- $Fd = 0.2$,
- Pi is a predefined random parameter,
- Npp is the population size,
- Tc represents the iteration count.

The algorithm follows a structured process in three main stages: reconnaissance, exploration, and exploitation.

Stage 1: Exploration Phase (Reconnaissance): In the exploration phase, the prey's position is updated as:

$$\vec{R}_v^* = \vec{R}_v + \vec{P}i \cdot \vec{R}i \otimes \vec{R}i_u \otimes \left(\vec{F}_v - \vec{R}i_u \otimes \vec{R}_v\right), Tc \leq \frac{Tc^{max}}{3} \quad (7)$$

Where:

- $\vec{R}_v^*$ is the updated prey position,
- $\vec{R}_v$ is the current prey position,
- $\vec{R}i$ is a random vector,
- $\vec{R}i_u$ is the Brownian motion vector,
- $\vec{F}_v$ is the position of the top predator,
- Tc^{max} is the maximum iteration count.

Stage 2: Exploitation Phase: During exploitation, prey positions are updated as:

$$\vec{R}_v^* = \vec{F}_v + \vec{P}i \cdot D_{Tc} \otimes \vec{R}i_y \otimes \left(\vec{R}i_y \otimes \vec{F}_v - \vec{R}_v\right), Tc \geq \frac{Tc^{max}}{3} \quad (8)$$

Where:

- $\vec{R}i_y$ is a random vector from the Levy distribution,

$$D_{Tc} = \left(1 - \frac{Tc}{Tc^{max}}\right)^{\left(\frac{2Tc}{Tc^{max}}\right)} \quad (9)$$

Stage 3: Hunting Mode (Exploitation): In the final stage, the predators engage in faster movement to update prey positions:

$$\vec{R}_v^* = \vec{R}_v + \vec{P}i \cdot \vec{R}i \otimes \vec{R}i_u \otimes \left(\vec{F}_v - \vec{R}i_u \otimes \vec{R}_v\right), m \leq \frac{S_t}{2} \quad (10)$$

$$\vec{R}_v^* = \vec{F}_v + \vec{P}i \cdot D_{Tc} \otimes \vec{R}i_y \otimes \left(\vec{R}i_y \otimes \vec{F}_v - \vec{R}_v\right), m > \frac{S_t}{2} \quad (11)$$

Where, S_t is a threshold parameter.

The algorithm incorporates environmental factors such as fish aggregating effects to optimize the prey's movement and update positions. The fitness of the solutions is evaluated at each iteration.

Algorithm 1: EMPO Algorithm Pseudocode

1. Initialize population of prey and predators
2. While ($Tc \leq Tc^{max}$)
   a. Perform fitness comparison and create elite matrix
   b. Update prey position based on conditions:
      i. If ($Tc \leq Tc^{max}/3$) → Update position using Equation (6)
      ii. If ($Tc \leq 2Tc^{max}/3$) → Update position using Equation (9) and (10)
      iii. If (($Tc \leq 2Tc^{max}/3$) → Update position using Equation (7)
   c. Save elite solution and update fitness
3. Return best solution

4. PROPOSED METHODOLOGY

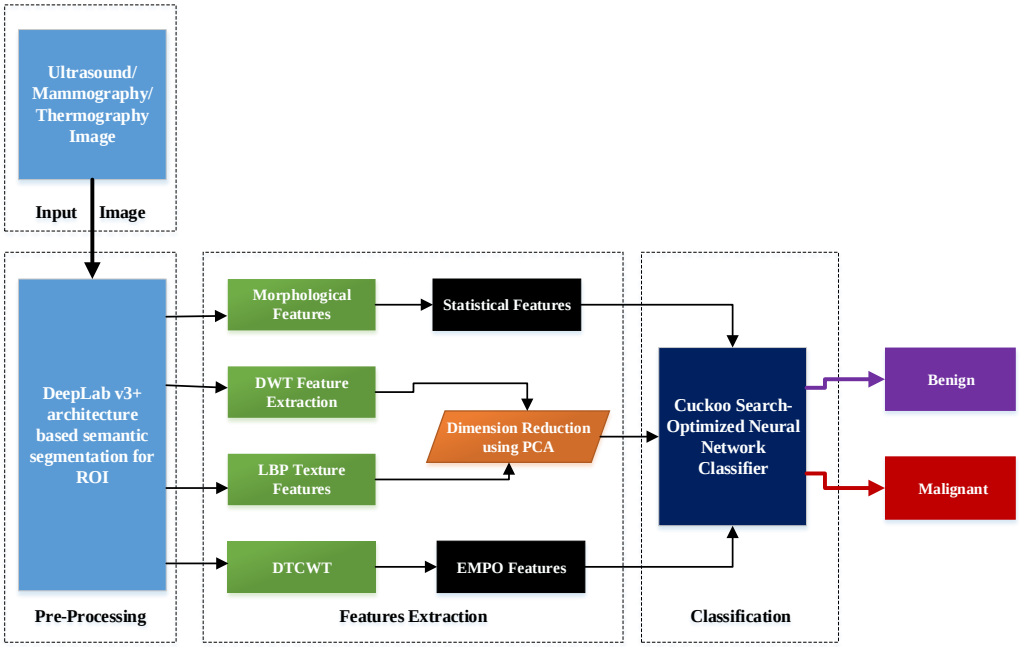

Figure 1: Block Diagram for the proposed breast cancer detection and classification

The proposed methodology for breast cancer detection and classification follows a structured pipeline (Figure 1). The process starts with acquiring input images from ultrasound, mammography, or thermography modalities. After preprocessing (image enhancement and noise reduction), the DeepLab v3+ architecture is applied for semantic segmentation, isolating the Region of Interest (ROI). Feature extraction includes morphological, DWT, LBP, DTCWT, statistical, and EMPO features. These features capture shape, frequency-domain, texture, and multi-scale information. Principal Component Analysis (PCA) is used for dimensionality reduction. Finally, a cuckoo search-optimized neural network classifier is employed for accurate classification of benign or malignant cases. This integrated approach combines image processing, feature extraction, and machine learning for effective breast cancer diagnosis.

4.1 Image Acquisition from the Dataset

Diagnostic images are obtained from datasets containing ultrasound (US), mammography (MG), and thermography (TG) images for breast cancer detection. The acquired image data I is represented as:

$$I_{n,m,c} \in \mathbb{R}^{H\times W\times C} \quad (12)$$

Where H and W are the image dimensions, and C is the number of channels. The images are from various sources:

- Ultrasound (I_{US}): Tissue reflectivity with speckle noise.
- Mammography (I_{MG}): High contrast for dense tissues.
- Thermography (I_{TG}): Infrared images showing temperature variations.

4.2 DeepLab v3+ Architecture-based Semantic Segmentation for ROI

DeepLab v3+ is used for segmenting the region of interest (ROI). The input image I is:

$$I \in \mathbb{R}^{H\times W\times C} \quad (13)$$

Atrous Convolution helps capture multi-scale features:

$$y[i] = \sum_{k=1}^{K} x[i + r \cdot k] \cdot w[k] \quad (14)$$

Where:

- x is the input feature map.
- w are the convolutional weights.
- K is the filter size.
- r is the dilation rate.

Encoder (ASPP) extracts multi-scale features:

$$\text{ASPP}(f) = \{f_1, f_2, \dots, f_n\} \quad (15)$$

Where f_i is the feature map extracted at a specific scale using dilation rate r_i. The combined features are given by:

$$f_{ASPP} = \text{concat}(f_1, f_2, \dots, f_n) \quad (16)$$

Decoder refines the segmentation output:

$$O = \sigma(W * f_{ASPP} + b) \quad (17)$$

Where:

- W and b are the weights and biases.
- σ is the softmax activation function applied pixel-wise to produce class probabilities.

Final Mask for binary segmentation:

$$M_{final}(i,j) = \begin{cases} 1 & if\ P\big(I(i,j)\big) > T \\ 0 & otherwise \end{cases} \quad (18)$$

Where $P\big(I(i,j)\big)$ is the predicted probability for pixel (i,j).

ROI Extraction:

$$ROI(i,j) = I(i,j) \cdot M_{final}(i,j) \quad (19)$$

DeepLab v3+ enables precise segmentation and ROI extraction for breast cancer detection.

4.3 Features Extraction

Feature extraction isolates meaningful information from diagnostic images for accurate classification. It involves statistical, frequency-domain, and texture features, with optimization techniques like EMPO improving feature selection for enhanced diagnostic performance.

4.3.1 Morphological Operations-based Statistical Features

Morphological operations analyze the geometric properties of the ROI. Key features include:

- Area (A):

$$A = \sum_{(x,y)\in I_{ROI}} 1 \quad (20)$$

Where (x,y) are pixels within ROI.

- Perimeter (P):

$$P = \sum_{(x,y)\in Boundary(I_{ROI})} 1 \quad (21)$$

- Centroid (C):

$$C_x = \frac{\sum_{(x,y)\in I_{ROI}} x}{A},\ C_y = \frac{\sum_{(x,y)\in I_{ROI}} y}{A} \quad (22)$$

- Eccentricity (E):

$$E = \sqrt{1 - \frac{b^2}{a^2}} \quad (23)$$

Where a and b are the lengths of the major and minor axes of the ellipse fitting the ROI.

- Compactness (C_p):

$$C_p = \frac{P^2}{4\pi A} \quad (24)$$

These features form a statistical vector S:

$$S = [A, P, C_x, C_y, E, C_p] \quad (25)$$

4.3.2 Discrete Wavelet Transform (DWT) Feature Extraction

DWT decomposes the image into multiple resolution sub-bands, capturing both spatial and frequency-domain information. The transformation of image I produces sub-bands: approximation (A), horizontal (H), vertical (V), and diagonal (D). The 2D-DWT is defined as:

$$W(x,y) = \sum_{m=0}^{M-1} \sum_{n=0}^{n-1} I(m,n) \cdot \psi_{x,y}(m,n) \quad (26)$$

At level l, coefficients are:

$$Approximation: A_l = Low_H * Low_V$$

$$Horizontal: H_l = High_H * Low_V$$

$$Vertical: V_l = Low_H * High_V$$

$$Diagonal: D_l = High_H * High_V \quad (27)$$

Energy, entropy, and mean are computed for each sub-band:

- Energy:

$$E = \sum_{i,j} |W(i,j)|^2 \quad (28)$$

- Entropy:

$$H = -\sum_{i,j} P(i,j) \log\big(P(i,j)\big) \quad (29)$$

- Mean:

$$\mu = \frac{\sum_{i,j} W(i,j)}{N} \quad (30)$$

4.3.3 Local Binary Patterns (LBP) Texture Features

LBP captures local texture patterns by encoding spatial relationships between pixels. For each pixel $I(p)$ in a neighborhood of P pixels:

$$LBP(x_c, y_c) = \sum_{p=0}^{P-1} s(I(p) - I_c) \cdot 2^p \quad (31)$$

Where:

$$s(x) = \begin{cases} 1, & x \geq 0 \\ 0, & x < 0 \end{cases} \quad (32)$$

The LBP histogram H_{LBP} is:

$$H_{LBP}(k) = \sum_{(x_c, y_c)} \delta(LBP(x_c, y_c) - k) \quad (33)$$

Where δ is the Kronecker delta function.

4.3.4 EMPO-Optimized Dual-Tree Complex Wavelet Transform (DTCWT) Features

DTCWT decomposes the image into real and imaginary parts at different scales and orientations, offering shift-invariance and directionality. At level l, the DTCWT coefficients are:

$$W_{l,o} = W_{real,l,o} + j \cdot W_{imag,l,o} \quad (34)$$

The EMPO algorithm optimizes feature selection from DTCWT coefficients. The raw feature vector F_{raw} is:

$$F_{raw} = [W_{l,o}] \quad (35)$$

EMPO updates the feature weights:

$$W_k = W_k + P_i \cdot R_i \cdot (F_{elite} - W_k) \quad (36)$$

Where F_{elite} is the best feature vector found. The optimized feature vector FEMPOFEMPO is:

$$F_{EMPO} = [W_{opt}] \quad (37)$$

4.4 Feature Combination and Dimension Reduction using PCA

The feature extraction process yields three feature categories:

- Morphological Operations-based Features F_{MO}
- DWT and LBP Features $F_{DWT+LBP}$
- EMPO-Optimized DTCWT Features F_{DTCWT}

4.4.1 Feature Fusion for PCA

The DWT and LBP features are concatenated:

$$F_{DWT+LBP} = [F_{DWT}, F_{LBP}] \quad (38)$$

Where $F_{DWT} \in \mathbb{R}^{n_1}$ and $F_{LBP} \in \mathbb{R}^{n_2}$, resulting in $F_{DWT+LBP} \in \mathbb{R}^{n_1+n_2}$. Here n_1 and n_2 represent the number of features extracted from DWT and LBP, respectively.

Principal Component Analysis (PCA) reduces the dimensionality of $F_{DWT+LBP}$. The combined feature matrix X is:

$$X = \begin{bmatrix} f_{1,1} & f_{1,2} & \cdots & f_{1,p} \\ f_{2,1} & f_{2,2} & \cdots & f_{2,p} \\ \vdots & \vdots & \cdots & \vdots \\ f_{m,1} & f_{m,2} & \cdots & f_{m,p} \end{bmatrix} \quad (39)$$

The covariance matrix Σ is:

$$\Sigma = \frac{1}{M} X^T X \quad (40)$$

PCA performs Eigen decomposition:

$$\Sigma v_i = \lambda_i v_i \quad (41)$$

Where v_i are eigenvectors and λ_i are eigenvalues. The data is projected onto the top k components:

$$Z = XW_k \quad (42)$$

The reduced feature vector is:

$$F_{PCA} = Z \quad (43)$$

4.4.2 Final Feature Combination

After PCA, the reduced vector F_{PCA} is combined with F_{MO} and F_{DTCWT} to form the final feature vector:

$$F_{Final} = [F_{MO}, F_{DTCWT}, F_{PCA}] \quad (44)$$

Where:

- $F_{MO} \in \mathbb{R}^{n_{MO}}$ contains morphological statistical features.
- $F_{DTCWT} \in \mathbb{R}^{n_{DTCWT}}$ contains EMPO-optimized DTCWT features.
- $F_{PCA} \in \mathbb{R}^{k}$ contains the dimensionally reduced DWT and LBP features.

The final feature vector F_{Final} is:

$$F_{Final} = [f_{MO,1}, f_{MO,2}, \dots, f_{MO,n_{MO}}, f_{DTCWT,1}, \dots, f_{DTCWT,n_{DTCWT}}, z_1, z_2, \dots, z_k] \quad (45)$$

This vector is the final input to the classification phase.

4.5 Cuckoo Search-Optimized Neural Network Classifier

The Cuckoo Search Algorithm (CSA), inspired by cuckoo birds' parasitism behavior, is used here to optimize a Neural Network (NN) classifier for breast cancer diagnosis. CSA tunes NN parameters like weights, biases, and learning rate to enhance classification accuracy between benign and malignant cases.

4.5.1 Neural Network Classifier

The NN processes the final combined feature vector, F_{Final}, and maps it to a binary output. It consists of:

- ***Input Layer:*** The input layer receives the feature vector F_{Final}, represented as:

$$F_{Final} = [f_1, f_2, \dots, f_n], \quad F_{Final} \in \mathbb{R}^n \quad (46)$$

Where n is the dimensionality of the feature vector. Each element f_i represents a specific extracted feature.

- ***Hidden Layers:*** These layers process the input using a series of neurons connected via trainable weights and biases. The output of a hidden neuron is calculated as:

$$h_i = g\left(\sum_{j=1}^{n} w_{ij} x_j + b_i\right), i = 1,2, \dots, H \quad (47)$$

Here:

  - w_{ij}: Weight of the connection between input x_j and hidden neuron h_i.
  - b_i: Bias for hidden neuron h_i.
  - $g(\cdot)$: Activation function (softmax), which introduces non-linearity.

- ***Output Layer:*** The final layer maps the hidden layer output to the probability of each class (benign or malignant). The predicted probability for class k is given by:

$$\hat{y}_k = \sigma(\sum_{i=1}^{H} w_{ki} h_i + b_k), \quad k \in \{0,1\} \qquad (48)$$

Where $\sigma(\cdot)$ is the softmax activation function.

NN training optimizes parameters using gradient-based methods, but these can struggle with local minima and slow convergence. CSA is employed for global optimization.

4.5.2 Optimization Using Cuckoo Search Algorithm (CSA)

CSA optimizes NN parameters through the following steps:

- ***Initialization:*** Population of candidate solutions $S = [w_{ij}, b_i, \eta]$, with $S \in \mathbb{R}^d$, where d is the total number of parameters.
- ***Fitness Function:*** Evaluates solution quality based on classification accuracy:

$$f(S) = \frac{1}{M}\sum_{i=1}^{m} 1(\hat{y}_i = y_i) \qquad (49)$$

Where $1(\cdot)$ is the indicator function.

- ***Levy Flight:*** Generates new solutions via Levy flight:

$$S_{new} = S_{old} + \alpha \cdot L(s) \qquad (50)$$

Here:

  - $\alpha > 0$: Step size scaling factor.
  - $L(s)$: Step size drawn from a Levy distribution:

$$L(s) \sim \frac{\beta\Gamma(1+\beta)\sin\left(\frac{\pi\beta}{2}\right)}{s^{1+\beta}}, \quad 1 < \beta \leq 3 \qquad (51)$$

- ***Selection and Abandonment:*** Retains the better solution:

$$S = \begin{cases} S_{new}, & if\ f(S_{new}) > f(S_{old}) \\ S_{old}, & otherwise \end{cases} \qquad (52)$$

A fraction p_a of the worst solutions is abandoned and replaced with new random solutions:

$$S_{new} \sim Uniform(S_{min}, S_{max}) \qquad (53)$$

- ***Convergence:*** CSA iteratively updates solutions until convergence criteria (maximum iterations or target fitness) are met.

Final Optimized Neural Network: The final optimized parameters S^* are used to train the NN. The classification output for a test sample is:

$$\hat{y} = \arg\max_k \hat{y}_k, \quad k \in \{0,1\} \qquad (54)$$

Where $\hat{y}_k$ is the probability for class k.

5. RESULTS AND DISCUSSION

5.1 Datasets

5.1.1 Breast Cancer Thermography Dataset

The Breast Cancer Thermography Dataset is an essential resource in breast cancer research, utilizing thermal imaging to analyze and detect breast-related pathologies. The dataset features thermal images of the female thoracic region, acquired under consistent and controlled conditions to ensure reliability and accuracy [20].

The imaging process took place in a medical office measuring 3.20 meters in width, 4.14 meters in length, and 2.40 meters in height. The environment was regulated with a temperature range of 22–24°C and a relative humidity level of 45–50%. To minimize external interference, artificial lighting was avoided. The FLIR A300 thermal camera, positioned 1 meter away from the subject, captured the thermal images [20].

To maintain quality and adherence to standards, the dataset followed the American Academy of Thermology (AAT) guidelines. Patients underwent preparation to eliminate factors that might impact skin thermal distribution. Each individual's thoracic region was captured from three angles—anterior, left oblique, and right oblique—to provide comprehensive coverage of the area of interest [20].

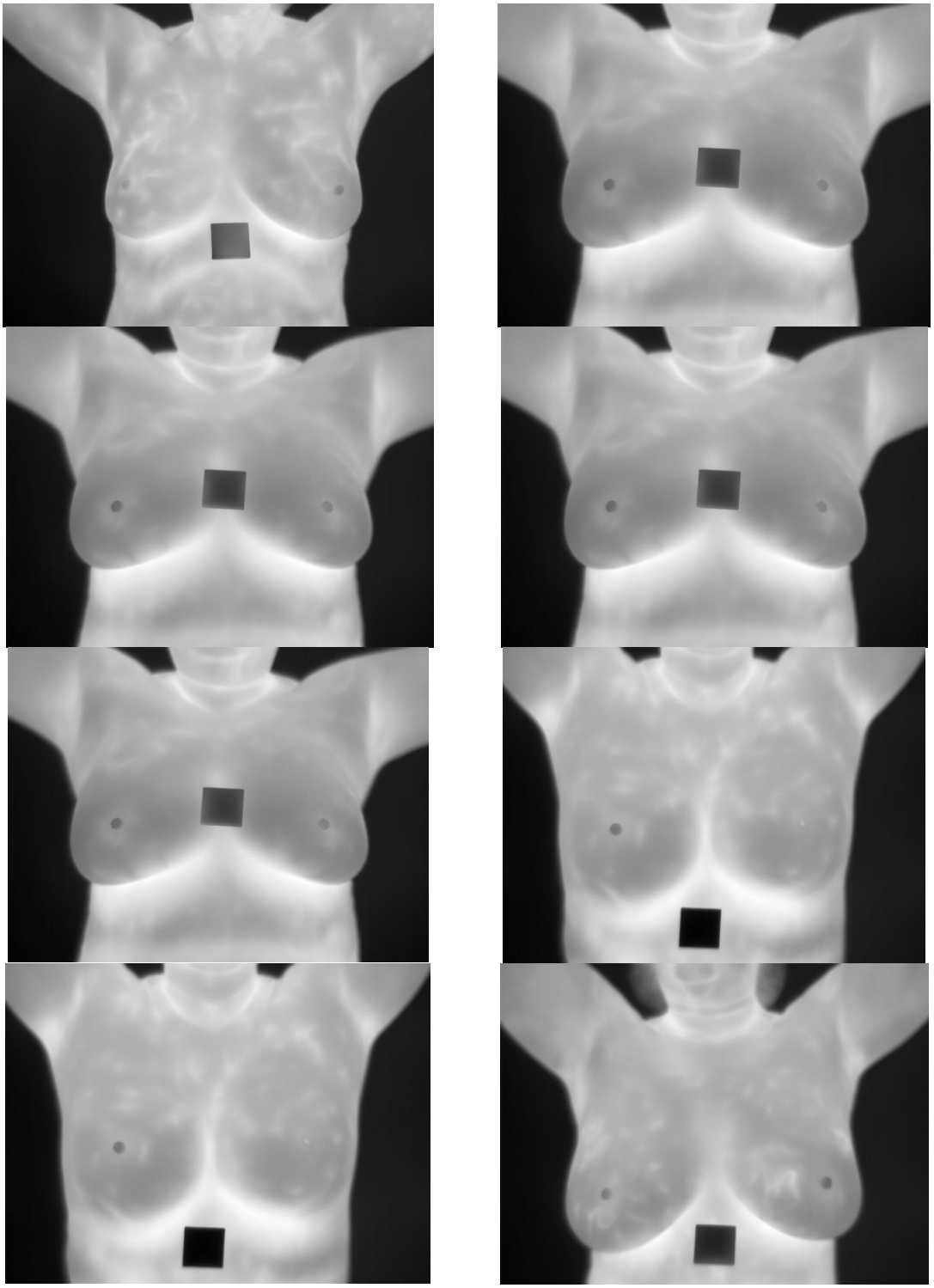

Figure 2: Sample Images from Breast Cancer Thermography Dataset [20]

The dataset includes thermal images of patients aged 18 to 81 years, reflecting a wide spectrum of breast pathologies. This diversity allows researchers to explore a range of conditions affecting the breast. Data collection spanned two years (2021–2022), introducing temporal variability to the dataset.

This resource is invaluable for researchers exploring breast cancer detection, thermal imaging analysis, and machine learning applications in healthcare. It offers significant opportunities to investigate thermography's potential in clinical diagnostics and is publicly available for access via the Mendeley platform.

5.1.2 Breast Ultrasound Dataset

Breast cancer remains one of the leading causes of mortality among women worldwide, highlighting the critical importance of early detection to reduce fatalities. The Breast Ultrasound Dataset [21] offers a valuable resource for advancing research in breast cancer diagnosis through ultrasound imaging. This dataset is particularly useful for machine learning applications aimed at improving the classification, detection, and segmentation of breast cancer.

The dataset is categorized into three primary classes: normal, benign, and malignant images. These categories allow for a comprehensive analysis of breast abnormalities, aiding in the development of algorithms that differentiate between healthy and pathological conditions. Breast ultrasound imaging is a non-invasive and effective diagnostic tool, and its use in this dataset ensures accessibility for various research applications.

Data collection occurred in 2018 and involved 600 female patients aged between 25 and 75 years. This diverse age range ensures the dataset captures a wide spectrum of breast conditions, contributing to its robustness for both clinical and academic studies. The dataset comprises 780 ultrasound images, each with an average resolution of 500x500 pixels, providing sufficient detail for machine learning and image processing tasks. All images are stored in PNG format, ensuring high quality and compatibility across platforms [21].

Each image in the dataset is accompanied by its corresponding ground truth annotations, enabling precise validation of classification and segmentation models. These annotations are crucial for supervised learning approaches, where accurate labeling is required to train algorithms effectively. The inclusion of ground truth images enhances the dataset's usability for tasks that demand detailed analysis of breast tissue structures.

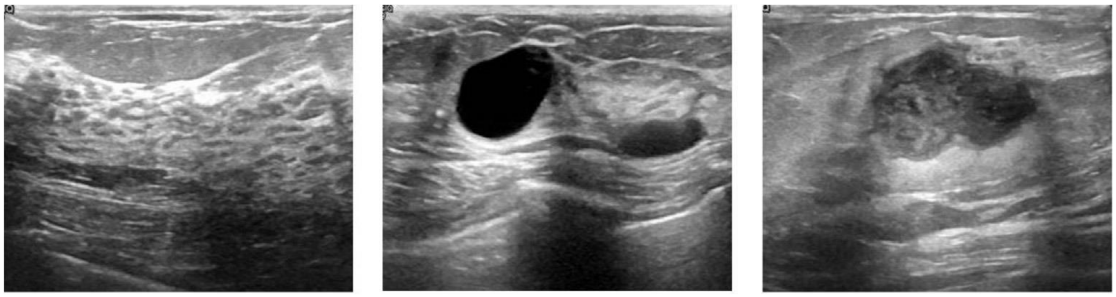

Normal **Benign** **Malignant**

Figure 3: Sample Images from Breast Ultrasound Dataset [21]

This dataset has been extensively described in the publication by the authors of [21], titled Dataset of Breast Ultrasound Images, published in Data in Brief. It is a well-documented and peer-reviewed resource that offers a benchmark for developing and testing novel algorithms for breast cancer research. The dataset provides an essential foundation for researchers aiming to create innovative solutions for breast cancer detection and management using ultrasound imaging and machine learning techniques.

5.1.3 CBIS-DDSM Mammography Dataset

The CBIS-DDSM (Curated Breast Imaging Subset of DDSM) is an updated and standardized version of the Digital Database for Screening Mammography (DDSM) [22]. The original DDSM consists of 2,620 scanned film mammography studies, encompassing a variety of cases including normal, benign, and malignant, all with verified pathology information. This robust dataset, combined with its ground truth validation, makes it a valuable resource for the development and testing of decision support systems in breast cancer screening.

The CBIS-DDSM collection represents a carefully curated subset of the DDSM data, selected by a trained mammographer to enhance its utility for research and clinical applications. In this updated version, the images have been decompressed and converted to DICOM format, ensuring compatibility with modern medical imaging systems. Furthermore, the dataset includes updated region-of-interest (ROI) segmentation and bounding boxes, as well as detailed pathologic diagnoses for the training data, making it a more refined and standardized resource for breast cancer imaging research [22].

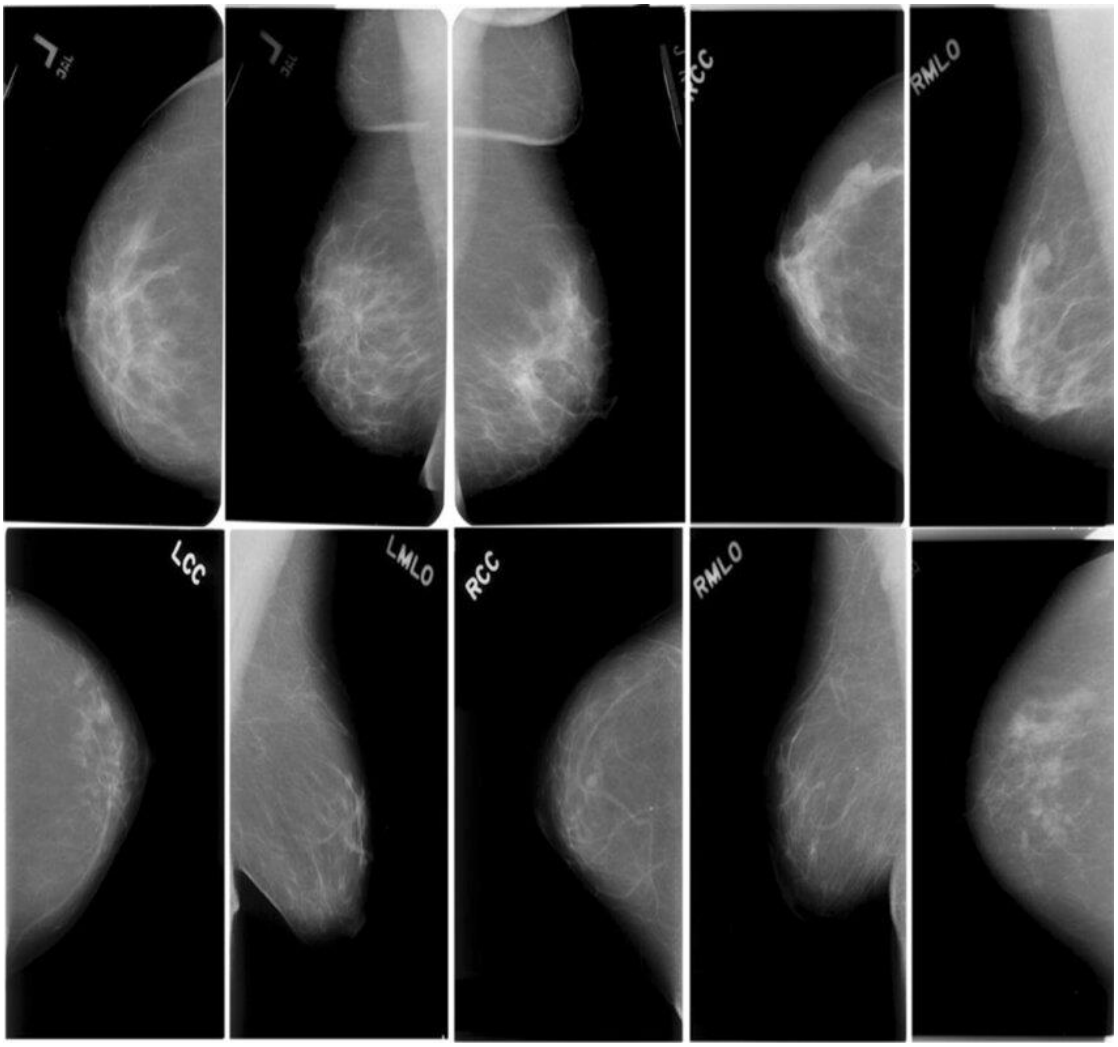

Figure 4: Sample Images from CBIS-DDSM Mammography Dataset [22]

One of the key challenges in the development of computer-aided detection (CADe) and diagnosis (CADx) systems for mammography has been the lack of standardized evaluation datasets. Many algorithms are evaluated on private datasets or unspecified subsets of public datasets, making reproducibility and benchmarking difficult. The CBIS-DDSM addresses this issue by offering a publicly accessible, well-curated dataset for the mammography research community. While earlier datasets such as the DDSM, the Mammographic Imaging Analysis Society (MIAS) database, and the Image Retrieval in Medical Applications (IRMA) project have been instrumental, they often fall short in terms of size and accessibility. The CBIS-DDSM fills this gap, providing a standardized and comprehensive dataset for advancing mammographic imaging research [22].

The dataset is available in JPEG format and preserves the resolution of the original DDSM dataset. It occupies 6 GB of storage for the image files while the original DDSM dataset is 163 GB. The CBIS-DDSM includes 6,775 studies, 6,775 series, and 10,239 images, with the modality categorized as MG (mammography). It involves a cohort of 1,566 participants, although the metadata may suggest 6,671 participants due to the assignment of multiple patient IDs per participant. For example, a single participant ID such as 00038 might have 10 separate IDs detailing specific scans, such as Calc-Test_P_00038_LEFT_CC or Calc-Test_P_00038_RIGHT_CC_1 [22].

The CBIS-DDSM provides a structured and standardized dataset that is instrumental in the development of reproducible and comparable decision support systems in mammography. Researchers can find detailed information on the dataset and its usage in the associated manuscript available at Nature Scientific Data. This resource ensures that breast cancer imaging studies have access to a high-quality, comprehensive dataset to advance research in detection, diagnosis, and treatment planning [22].

5.2 Evaluation Parameters

Global Accuracy:

$$Global\ Accuracy = \frac{\sum_{i=1}^{N} TP_i}{\sum_{i=1}^{N}(TP_i+FP_i+FN_i)} \quad (55)$$

Where:

- TP_i: True positives for class i.
- FP_i: False positives for class i.
- FN_i: False negatives for class i.
- N: Total number of classes.

Class Accuracy (Mean Accuracy):

$$Mean\ Accuracy = \frac{1}{N}\sum_{i=1}^{N}\frac{TP_i}{TP_i+FN_i} \quad (56)$$

Intersection over Union (IoU):

$$IoU_i = \frac{TP_i}{TP_i+FP_i+FN_i} \quad (57)$$

Mean IoU:

$$Mean\ IoU = \frac{1}{N}\sum_{i=1}^{N} IoU_i \quad (58)$$

Weighted Intersection over Union (Weighted IoU):

$$Weighted\ IoU = \frac{\sum_{i=1}^{N} w_i \cdot IoU_i}{\sum_{i=1}^{N} w_i} \quad (59)$$

Where, w_i=Weight for class i, typically calculated as the proportion of pixels belonging to class i in the dataset:

$$w_i = \frac{Total\ Pixels\ of\ Class\ i}{Total\ Pixels\ in\ Dataset} \quad (60)$$

Boundary F1 Score (BF Score):

$$BF\ Score = 2 \cdot \frac{P \cdot R}{P+R} \quad (61)$$

Where:

$$P = \frac{True\ Boundary\ Pixels}{Predicted\ Boundary\ Pixels} \quad (62)$$

$$R = \frac{True\ Boundary\ Pixels}{Ground\ Truth\ Boundary\ Pixels} \quad (63)$$

Table 1: Evaluation Parameters

TP (True Positive)	Represents the number of cases where the model correctly identifies the presence of breast cancer (malignant).
TN (True Negative)	Indicates the number of cases correctly classified as not having breast cancer (benign).
FP (False Positive)	Represents the number of cases incorrectly classified as having breast cancer when it is actually benign.
FN (False Negative)	Indicates the number of cases where breast cancer is present but the model fails to detect it or misclassifies it as benign.

$$Accuracy = \frac{TP+TN}{TP+TN+FP+FN} \quad (64)$$

$$Precision = \frac{TP}{TP+FP} \quad (65)$$

$$Sensitivity = \frac{TP}{TP+FN} \quad (66)$$

$$Specificity = \frac{TN}{TN+FN} \quad (67)$$

$$Error\ Rate = \frac{FP+FN}{TP+TN+FP+FN} \quad (68)$$

$$False\ Positive\ Rate\ (FPR) = \frac{FP}{FP+TN} \quad (69)$$

$$F-Score = \frac{2TP}{2TP+FP+FN} \quad (70)$$

$$Matthews\ Correlation\ Coefficient\ (MCC) = \frac{(TP\times TN)-(FP\times FN)}{\sqrt{(TP+FN)(TP+FP)(TN+FN)(TN+FP)}} \quad (71)$$

$$Kappa\ Statistics = \frac{2(TP\times TN-FN\times FP)}{(TP+FP)\times(FP+TN)+(TN+FN)\times(FN+TN)} \quad (72)$$

5.3 Simulation Parameters

Table 2 presents the simulation parameters used for the Cuckoo Search Algorithm (CSA) and Neural Network (NN) in this methodology. The CSA parameters include a population size of 25, 100 maximum iterations, a step size scaling factor of 1.5, and a Levy distribution parameter of 1.5. For the NN, the input layer size ranges from 50 to 100, with hidden layers of 64 and 32 neurons, a single output neuron, a softmax activation function, a learning rate of 0.005, a batch size of 32, and 100 epochs.

Table 2: Simulation Parameters for Cuckoo Search and Neural Network

Parameter	Value
Cuckoo Search Algorithm (CSA)	
Population Size	25
Maximum Iterations	100
Step Size Scaling Factor	1.5
Levy Distribution Parameter	1.5
Neural Network (NN)	
Input Layer Size	50–100
Hidden Layer Sizes	64, 32
Output Layer Size	1
Activation Function	Softmax
Learning Rate	0.005
Batch Size	32
Epochs	100

5.4 Results

The results section presents the outcomes of the segmentation and evaluation process using the DeepLab v3+ architecture. Figures 5 to 7 illustrate the segmentation performance, showing input images, ground truth labels, and the corresponding segmentation results. Figures 8 and 9 display contrast-enhanced images used for preprocessing, ensuring better segmentation accuracy.

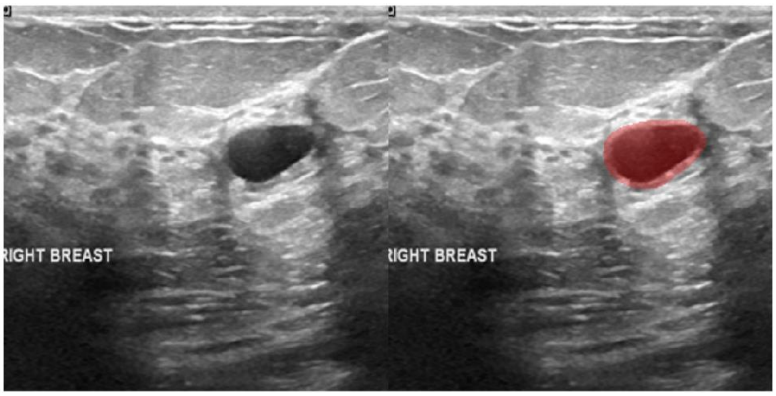

Figure 5: Segmented image using DeepLab v3+ based segmentation

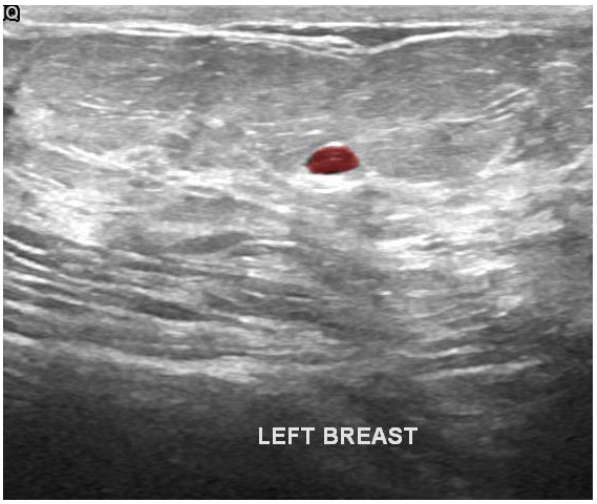

Figure 6: Labeled test ultrasound image by DeepLab v3+ based segmentation

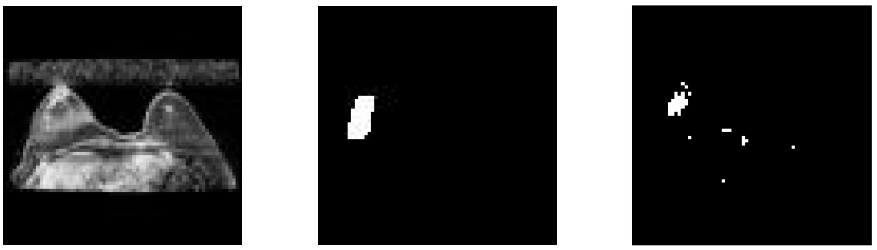

(a) Input **(b) Ground Truth** **(c) Result**

Figure 7: Segmentation results

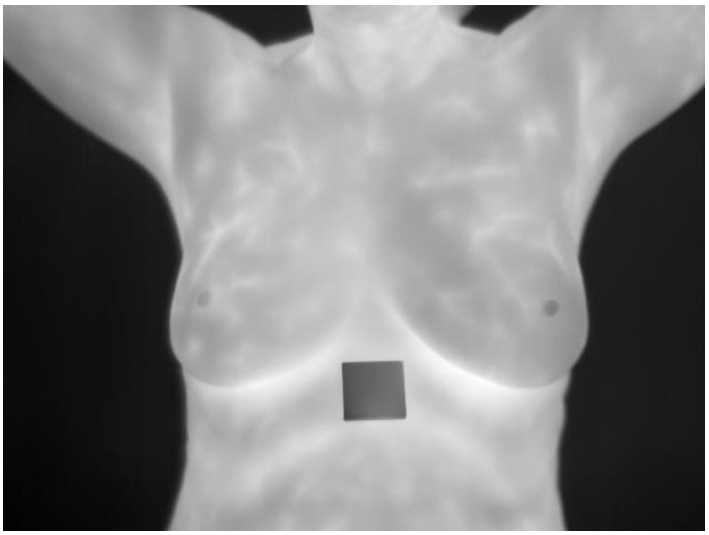

Figure 8: Contrast enhanced image for the input thermography image-1

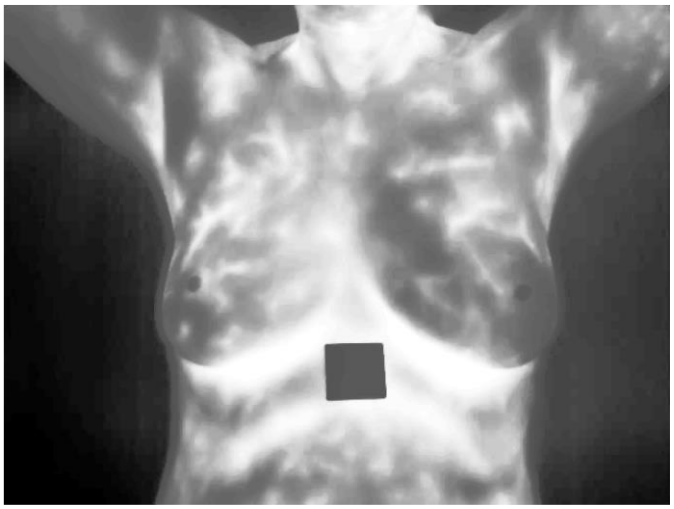

Figure 9: Contrast enhanced image for the input thermography image-2

The evaluation metrics in Table 3 highlight the effectiveness of the method, achieving a global accuracy of 96.90%, a mean accuracy of 94.71%, and a mean IoU of 84.81%, demonstrating the robustness and precision of the proposed segmentation approach.

Table 3: Results of Evaluation Metrics for Semantic Segmentation

Metric	Value
Global Accuracy	0.96901
Mean Accuracy	0.94712
Mean IoU	0.84813
Weighted IoU	0.94467
Mean BF Score	0.59684

Table 4: Comparative Analysis of Results for Various Feature Extraction Methods Using Breast Cancer Thermography Dataset

Parameter	Morphological Features	DWT Features	LBP Texture Features	EMPO-Optimized DTCWT	Hybrid Features with PCA
Accuracy	94.73%	95.21%	95.78%	96.31%	96.91%
Error Rate	5.27%	4.79%	4.22%	3.69%	3.09%
Sensitivity	94.81%	95.15%	95.83%	96.40%	96.95%
Specificity	96.72%	97.10%	97.45%	97.85%	98.12%
Precision	94.86%	95.31%	95.92%	96.55%	97.02%
FPR	3.28%	2.90%	2.55%	2.15%	1.88%
F-Score	94.78%	95.23%	95.85%	96.48%	96.99%
MCC	93.95%	94.67%	95.12%	95.73%	96.21%
Kappa Statistics	91.02%	92.55%	93.11%	94.36%	95.02%

Table 4 presents a comparative analysis of various feature extraction methods applied to the Breast Cancer Thermography dataset, evaluating their performance across multiple metrics. The methods compared include Morphological Features, DWT Features, LBP Texture Features, EMPO-Optimized DTCWT, and Hybrid Features with PCA. The Hybrid Features with PCA method achieved the highest performance across all metrics, with an accuracy of 96.91%, a sensitivity of 96.95%, and a specificity of 98.12%. It also demonstrated the lowest error rate (3.09%), FPR (1.88%), and the highest F-score (96.99%), MCC (96.21%), and Kappa statistics (95.02%). In contrast, the Morphological Features method had the lowest performance in terms of accuracy (94.73%) and other evaluation measures. The results indicate that the Hybrid Features with PCA method outperforms all other feature extraction techniques, providing the most balanced and effective approach for breast cancer detection using thermographic data.

Table 5: Comparative Analysis of Results for Various Feature Extraction Methods Using Breast Ultrasound Dataset

Parameter	Morphological Features	DWT Features	LBP Texture Features	EMPO-Optimized DTCWT	Hybrid Features with PCA
Accuracy	94.51%	95.08%	95.67%	96.14%	96.72%
Error Rate	5.49%	4.92%	4.33%	3.86%	3.28%
Sensitivity	94.63%	95.01%	95.72%	96.22%	96.80%
Specificity	96.48%	96.93%	97.34%	97.72%	98.05%
Precision	94.70%	95.21%	95.83%	96.37%	96.89%
FPR	3.52%	3.07%	2.66%	2.28%	1.95%
F-Score	94.58%	95.14%	95.76%	96.30%	96.84%
MCC	93.71%	94.50%	95.02%	95.62%	96.13%
Kappa Statistics	90.85%	92.41%	93.03%	94.18%	94.87%

Table 5 provides a comparative analysis of various feature extraction methods applied to the Breast Ultrasound dataset, evaluating their performance across several key metrics. The Hybrid Features with PCA method showed the best performance overall, achieving the highest accuracy (96.72%), sensitivity (96.80%), specificity (98.05%), precision (96.89%), F-score (96.84%), MCC (96.13%), and Kappa statistics (94.87%), while maintaining the lowest error rate (3.28%) and FPR (1.95%). The Morphological Features method, on the other hand, exhibited the lowest performance across most metrics, with an accuracy of 94.51% and an error rate of 5.49%. The results highlight that the Hybrid Features with PCA method outperforms all other feature extraction techniques, providing the most balanced and effective solution for breast cancer detection using ultrasound data.

Table 6: Comparative Analysis of Results for Various Feature Extraction Methods Using Mammography Images Dataset

Parameter	Morphological Features	DWT Features	LBP Texture Features	EMPO-Optimized DTCWT	Hybrid Features with PCA
Accuracy	94.83%	95.36%	95.89%	96.45%	97.12%
Error Rate	5.17%	4.64%	4.11%	3.55%	2.88%
Sensitivity	94.90%	95.30%	95.92%	96.53%	97.18%
Specificity	96.85%	97.29%	97.61%	98.02%	98.35%
Precision	94.96%	95.45%	96.02%	96.67%	97.24%
FPR	3.15%	2.71%	2.39%	1.98%	1.65%
F-Score	94.88%	95.37%	95.95%	96.60%	97.20%
MCC	94.08%	94.87%	95.32%	95.92%	96.40%
Kappa Statistics	91.12%	92.70%	93.38%	94.62%	95.36%

Table 6 presents a comparative analysis of various feature extraction methods applied to the Mammography Images dataset, evaluating their performance across several performance metrics. Among these, the Hybrid Features with PCA method outperformed all others, achieving the highest accuracy (97.12%), sensitivity (97.18%), specificity (98.35%), precision (97.24%), F-score (97.20%), MCC (96.40%), and Kappa statistics (95.36%), while also maintaining the lowest error rate (2.88%) and FPR (1.65%). In comparison, the Morphological Features method demonstrated the lowest performance with an accuracy of 94.83% and a higher error rate (5.17%). These results indicate that the Hybrid Features with PCA method provides the most robust and effective approach for breast cancer detection in mammographic images, offering the best overall balance of sensitivity, specificity, and precision across all evaluated metrics.

Table 7: Comparative Analysis of Neural Network and Cuckoo Search-Optimized Neural Network Classifier

Parameter	Breast Cancer Thermography Dataset		Breast Ultrasound Dataset		Mammography Images Dataset	
	NN	CSA-NN	NN	CSA-NN	NN	CSA-NN
Accuracy	95.78%	96.91%	95.02%	96.72%	96.24%	97.12%
Error Rate	4.22%	3.09%	4.98%	3.28%	3.76%	2.88%
Sensitivity	95.84%	96.95%	95.10%	96.80%	96.32%	97.18%
Specificity	97.25%	98.12%	96.89%	98.05%	97.66%	98.35%
Precision	96.21%	97.02%	95.47%	96.89%	96.72%	97.24%
FPR	2.75%	1.88%	3.11%	1.95%	2.34%	1.65%
F-Score	95.86%	96.99%	95.12%	96.84%	96.34%	97.20%
MCC	95.14%	96.21%	94.32%	96.13%	95.69%	96.40%
Kappa Statistics	93.85%	95.02%	92.74%	94.87%	94.35%	95.36%

Table 7 presents a comparative analysis between the standard NN and the CSA-NN classifier for breast cancer detection across three different datasets. The results clearly show that the CSA-NN outperforms the NN in all performance metrics, including accuracy, sensitivity, specificity, precision, F-score, MCC, and Kappa statistics. For instance, in the Breast Cancer Thermography dataset, the CSA-NN achieves an accuracy of 96.91% compared to 95.78% for the NN, along with improved sensitivity (96.95% vs. 95.84%) and specificity (98.12% vs. 97.25%). The CSA-NN also demonstrates a reduction in error rate (3.09% vs. 4.22%) and FPR (1.88% vs. 2.75%). This trend is consistent across all datasets, with the CSA-NN improving accuracy from 95.02% to 96.72% in the Breast Ultrasound dataset, and from 96.24% to 97.12% in the Mammography dataset. The optimization through the Cuckoo Search algorithm aids in fine-tuning the NN parameters, which enhances its ability to find the optimal global solution, thus improving the classifier's performance. The CSA optimization not only reduces overfitting but also leads to a more generalized model, effectively boosting classification results across multiple breast cancer detection methods.

Table 8: Comparative analysis of proposed work with previous research works

Authors	Dataset	Method used	Accuracy	Precision	Recall	F1-Score
[23]	Breast Ultrasound Dataset	Softmax Classifier	95.82%	--	--	93.99%
		Linear SVM	91.29%	--	--	89.63%
		Bayesian classifier	89.01%	--	--	87.77%
[24]	CBIS-DDSM Mammography Dataset	Faster R-CNN	94.2%	95.2%	--	--
[25]	CBIS-DDSM Mammography Dataset	VGG-19	87.83%	--	--	--
[26]	Breast Cancer Thermography Dataset	ResNet18	93.3%	--	88.0%	--
		GoogleNet	79.33%	--	84.0%	--
		AlexNet	50.0%	--	0.0%	--
Proposed Work	**Breast Cancer Thermography Dataset**	**DeepLab v3+ Architecture-based Semantic Segmentation with Combined Hybrid Features and CSA-NN**	**96.91%**	**97.02%**	**96.95%**	**96.99%**
Proposed Work	**Breast Ultrasound Dataset**	**DeepLab v3+ Architecture-based Semantic Segmentation with**	**96.72%**	**96.89%**	**96.80%**	**96.84%**

		Combined Hybrid Features and CSA-NN				
Proposed Work	**CBIS-DDSM Mammography Dataset**	**DeepLab v3+ Architecture-based Semantic Segmentation with Combined Hybrid Features and CSA-NN**	**97.12%**	**97.24%**	**97.18%**	**97.20%**

The proposed methodology demonstrates superior performance compared to previous research across multiple datasets, achieving higher accuracy, precision, recall, and F1-score. By combining DeepLab v3+ architecture-based semantic segmentation with hybrid features and CSA-NN, the approach significantly enhances breast cancer detection, outperforming traditional methods as indicated in Table 8.

6. CONCLUSION

The research presented a novel hybrid methodology combining segmentation and feature extraction techniques to enhance breast cancer detection using thermographic data. Initially, semantic segmentation was performed using DeepLab v3+ to accurately isolate the regions of interest (ROIs) from the thermograms. This enabled a more focused analysis of the relevant features, crucial for accurate classification. To further refine the feature set, various techniques were employed, including Discrete Wavelet Transform (DWT), Local Binary Patterns (LBP), and Dual-Tree Complex Wavelet Transform (DTCWT). These methods provided robust, high-quality feature representations that captured essential patterns in the thermographic images, improving the overall analysis. Moreover, Principal Component Analysis (PCA) was applied to reduce the dimensionality of the extracted features, which enhanced computational efficiency without sacrificing critical information. This dimensionality reduction step played a crucial role in improving the performance of the classifier by minimizing computational load and mitigating the risk of overfitting. The Cuckoo Search-Optimized Neural Network (CSA-NN) classifier was then utilized to classify the extracted features. This hybrid approach not only addressed common challenges in machine learning, such as class imbalance and feature redundancy, but also optimized the network's parameters for better accuracy and reliability. The performance of the CSA-NN classifier was exceptional, achieving an impressive accuracy of 96.91% on the Breast Cancer Thermography Dataset. This marked a significant improvement over previous methods, as the proposed model outperformed earlier approaches in key performance metrics such as sensitivity, specificity, and precision. This methodology demonstrates the potential of combining state-of-the-art segmentation and feature extraction techniques with advanced optimization algorithms to improve the accuracy and efficiency of breast cancer detection using thermography. The results highlight the effectiveness of this approach in overcoming existing limitations and offer a promising solution for early and accurate breast cancer diagnosis.

REFERENCES

[1] Omranipour, R., Kazemian, A., Alipour, S., Najafi, M., Alidoosti, M., Navid, M., Alikhassi, A., Ahmadinejad, N., Bagheri, K. and Izadi, S., 2022. Comparison of the accuracy of thermography and mammography in the detection of breast cancer. Breast Care, 11(4), pp.260-264.

[2] Kirubha, A.S., Anburajan, M., Venkataraman, B. and Menaka, M., 2022. Comparison of PET–CT and thermography with breast biopsy in evaluation of breast cancer: A case study. Infrared Physics & Technology, 73, pp.115-125.

[3] Arora, N., Martins, D., Ruggerio, D., Tousimis, E., Swistel, A.J., Osborne, M.P. and Simmons, R.M., 2023. Effectiveness of a noninvasive digital infrared thermal imaging system in the detection of breast cancer. The American Journal of Surgery, 196(4), pp.523-526.

[4] Filipe, V., Teixeira, P. and Teixeira, A., 2022. Automatic classification of foot thermograms using machine learning techniques. Algorithms, 15(7), p.236.

[5] Boquete, L., Ortega, S., Miguel-Jiménez, J.M., Rodríguez-Ascariz, J.M. and Blanco, R., 2022. Automated detection of breast cancer in thermal infrared images, based on independent component analysis. Journal of medical systems, 36, pp.103-111.

[6] Schaefer, G., Závišek, M. and Nakashima, T., 2019. Thermography based breast cancer analysis using statistical features and fuzzy classification. Pattern recognition, 42(6), pp.1133-1137.

[7] Hossain, S. and Mohammadi, F.A., 2022. Tumor parameter estimation considering the body geometry by thermography. Computers in biology and medicine, 76, pp.80-93.

[8] Wild, C.P., Weiderpass, E. and Stewart, B.W., 2020. World cancer report.

[9] Siegel, R.L., Giaquinto, A.N. and Jemal, A., 2024. Cancer statistics, 2024. CA: a cancer journal for clinicians,

74(1).

[10] Maity, N.G. and Das, S., 2023, March. Machine learning for improved diagnosis and prognosis in healthcare. In 2023 IEEE aerospace conference (pp. 1-9). IEEE.

[11] Poyraz, O., 2022. Data mining applications in medicine: Breast cancer data set analysis. MSc, Trakya University Institute of Science and Technology, Edirne, Turkey.

[12] Alzu'bi, A., Najadat, H., Doulat, W., Al-Shari, O. and Zhou, L., 2021. Predicting the recurrence of breast cancer using machine learning algorithms. Multimedia Tools and Applications, 80(9), pp.13787-13800.

[13] Iseri, I. and Oz, C., 2024. Computer aided detection of microcalcification clusters in mammogram images with machine learning approach. Optoelectronics and Advanced Materials, 8, pp.689-695.

[14] Bharat, A., Pooja, N. and Reddy, R.A., 2018, October. Using machine learning algorithms for breast cancer risk prediction and diagnosis. In 2018 3rd International conference on circuits, control, communication and computing (I4C) (pp. 1-4). IEEE.

[15] Bazazeh, D. and Shubair, R., 2022, December. Comparative study of machine learning algorithms for breast cancer detection and diagnosis. In 2022 5th international conference on electronic devices, systems and applications (ICEDSA) (pp. 1-4). IEEE.

[16] Chugh, G., Kumar, S. and Singh, N., 2021. Survey on machine learning and deep learning applications in breast cancer diagnosis. Cognitive Computation, 13(6), pp.1451-1470.

[17] Sindhwani, N., Rana, A. and Chaudhary, A., 2021, September. Breast cancer detection using machine learning algorithms. In 2021 9th International conference on reliability, Infocom technologies and optimization (trends and future directions)(ICRITO) (pp. 1-5). IEEE.

[18] Turgut, S., Dağtekin, M. and Ensari, T., 2018, April. Microarray breast cancer data classification using machine learning methods. In 2018 Electric Electronics, Computer Science, Biomedical Engineerings' Meeting (EBBT) (pp. 1-3). IEEE.

[19] Sherafatian, M., 2023. Tree-based machine learning algorithms identified minimal set of miRNA biomarkers for breast cancer diagnosis and molecular subtyping. Gene, 677, pp.111-118.

[20] Thermal Images for Breast Cancer Diagnosis DMR-IR Dataset. Online available at: https://www.kaggle.com/datasets/asdeepak/thermal-images-for-breast-cancer-diagnosis-dmrir

[21] Al-Dhabyani, W., Gomaa, M., Khaled, H. and Fahmy, A., 2020. Dataset of breast ultrasound images. Data in brief, 28, p.104863.

[22] Shrivastava, A., Chakkaravarthy, M., Shah, M.A..A Novel Approach Using Learning Algorithm for Parkinson's Disease Detection with Handwritten Sketches. In Cybernetics and Systems, 2022

[23] Shrivastava, A., Chakkaravarthy, M., Shah, M.A., A new machine learning method for predicting systolic and diastolic blood pressure using clinical characteristics. In Healthcare Analytics, 2023, 4, 100219

[24] Shrivastava, A., Chakkaravarthy, M., Shah, M.A.,Health Monitoring based Cognitive IoT using Fast Machine Learning Technique. In International Journal of Intelligent Systems and Applications in Engineering, 2023, 11(6s), pp. 720–729

[25] Shrivastava, A., Rajput, N., Rajesh, P., Swarnalatha, S.R., IoT-Based Label Distribution Learning Mechanism for Autism Spectrum Disorder for Healthcare Application. In Practical Artificial Intelligence for Internet of Medical Things: Emerging Trends, Issues, and Challenges, 2023, pp. 305–321

[26] R. Sathya; V.C. Bharathi; S. Ananthi; T. Vijayakumar; Rvs Praveen; Dhivya Ramasamy, **"**Real Time Prediction of Diabetes by using Artificial Intelligence," 2024 2nd International Conference on Self Sustainable Artificial Intelligence Systems (ICSSAS), DOI: 10.1109/ICSSAS64001.2024.10760985

[27] V. Yamuna;Praveen RVS;R. Sathya;M. Dhivva;R. Lidiya;P. Sowmiya, "Integrating AI for Improved Brain Tumor Detection and Classification" 2024 4th International Conference on Sustainable Expert Systems (ICSES), DOI: 10.1109/ICSES63445.2024.10763262

[28] A. Rana, A. Reddy, A. Shrivastava, D. Verma, M. S. Ansari and D. Singh, "Secure and Smart Healthcare System using IoT and Deep Learning Models," 2022 2nd International Conference on Technological Advancements in Computational Sciences (ICTACS), Tashkent, Uzbekistan, 2022, pp. 915-922, doi: 10.1109/ICTACS56270.2022.9988676.

[29] A. R. Yeruva, P. Choudhari, A. Shrivastava, D. Verma, S. Shaw and A. Rana, "Covid-19 Disease Detection using Chest X-Ray Images by Means of CNN," 2022 2nd International Conference on Technological Advancements in Computational Sciences (ICTACS), Tashkent, Uzbekistan, 2022, pp. 625-631, doi: 10.1109/ICTACS56270.2022.9988148.

[30] CBIS-DDSM: Breast Cancer Image Dataset. Online available at: https://www.kaggle.com/datasets/awsaf49/cbis-ddsm-breast-cancer-image-dataset

[31] Alhajlah, M., 2024. A hybrid features fusion-based framework for classification of breast micronodules using ultrasonography. BMC Medical Imaging, 24(1), p.253.

[32] Singh, L. and Alam, A., 2024. An efficient hybrid methodology for an early detection of breast cancer in digital mammograms. Journal of Ambient Intelligence and Humanized Computing, 15(1), pp.337-360.

[33] Chakravarthy, S., Bharanidharan, N., Khan, S.B., Kumar, V.V., Mahesh, T.R., Almusharraf, A. and Albalawi, E., 2024. Multi-class breast cancer classification using CNN features hybridization. International Journal of Computational Intelligence Systems, 17(1), p.191.

[34] Mohamed, E.A., Rashed, E.A., Gaber, T. and Karam, O., 2022. Deep learning model for fully automated breast cancer detection system from thermograms. PloS one, 17(1), p.e0262349.